Relevance of the $Co_{1−x}Ni_xWO_4$ wolframite-type mixed oxide compositions on the synthesis and catalytic properties of W-based carbides

Sergio L. González-Cortés [*],[1], Tian-Cun Xiao, Pedro M.F.J. Costa, Serbia M.A. Rodulfo-Baechler, Malcolm L.H. Green

Wolfson Catalysis Centre, Inorganic Chemistry Laboratory, University of Oxford, South Parks Road, Oxford OX1 3QR, UK

Abstract

A series of wolframite-type oxides ($Co_{1−x}Ni_xWO_4$) with various compositions was prepared by urea-matrix combustion method and subsequently carburized using a temperature-programmed reaction ($1\,^\circ C\,min^{-1}$) under a mixture of 10 vol.% C_2H_6/H_2, from room temperature to $700\,^\circ C$, to obtain a mixed Co, Ni and W carbide catalysts. The catalytic performance was evaluated in a continuous flow reactor using hydrodenitrogenation of pyridine as model reaction. The wolframite-type oxides and the carbide catalysts pre- and post-HDN reaction were characterized using elemental analysis, X-ray diffraction (XRD), laser Raman spectroscopy, thermogravimetric analysis (TGA), differential scanning calorimetric (DSC), transmission electron microscopy (TEM) and BET surface area measurements.

Urea-matrix combustion method is a convenient tool to prepare highly pure wolframite-type oxides, whose composition affects strongly the W-based carbide phase distribution and the HDN catalytic behaviour. At Ni compositions lower than Co contents the formation of Co_3W_3C and $β-W_2C$ carbides is favoured, whereas at Ni compositions greater than those of Co the main phases were Ni and $α-WC$. At intermediate composition ($Co_{0.5}Ni_{0.5}WC_x$) bimetallic and monometallic carbides were formed. The $CoWC_x$ bimetallic catalyst showed greater activity in the steady state than Ni-containing catalysts. The HDN active phase present in $CoWC_x$ is different than that present in the Ni-containing catalysts, that is, carbon–metal bond strength of the bimetallic carbide, for the former, and metal nickel or weak Ni−C bond, for the latter, play a very important role in the catalytic process.
© 2005 Elsevier B.V. All rights reserved.

Keywords: Wolframite-type mixed oxides; Carbide characterization; Co and Ni-containing W-based carbides; Pyridine-hydrodenitrogenation reaction

1. Introduction

Transition metal carbides have attracted considerable attention due to their similarities to noble metals. Recently, several methods have been developed for synthesizing high surface area carbide materials [1–4]. One of the most widely used methods is the temperature-programmed reaction (TPRe) method, developed by Boudart and co-workers [5–7]. This has been widely used to synthesize carbide catalysts for processes involving hydrogen transfer reactions, such as ammonia synthesis [8], hydrodenitrogenation (HDN) [9–12], hydrodesulfurization (HDS) [13,14], CO hydrogenation [15,16] and oxy-reforming of methane [17,18].

The mixed oxides generally employed as precursors of mixed carbides are synthesized by solid-state fusion requiring both high temperature and long time of calcination [10–12,19]. An alternative approach to produce highly pure mixed oxides in short period of calcination is the combustion synthesis [20], which relies on rapid, highly exothermic, solid flame reaction between a powder mixture to produce a

high temperature (upper 1100 K) over very short period of time. Under specific conditions, and following a short period of preheating, it is possible to obtain a self-propagating high temperature combustion wave that transforms the solid reactants to the final product of combustion. The product usually contains a high concentration of structural defects, which are beneficial as active centres in catalysis [21]. This material synthesis method has been used to prepare catalysts for deep oxidation of methane [22], oxidative coupling of methane [23], oxidation of carbon monoxide and reduction of NO [24,25].

Green and co-workers have studied the relationship of bimetallic carbide catalysts between structure and activity for the pyridine HDN reaction [10–12]. They have found that the addition of Co to Mo carbide [11] and of Ni to W carbide [12] had a significant effect on the structural, morphological and catalytic properties of the final carbide materials. However, many efforts have been mainly devoted to study the synthesis and catalytic properties of mono and bimetallic carbides but there has not been the same interest for trimetallic carbides, probably due to the difficult for preparing trimetallic mixed oxide precursors. Herein, it is reported the preparation of wolframite-type oxides (ABO_4) by urea-matrix combustion synthesis. The crystal structure of ABO_4 (A = Co (II) and/or Ni (II), and B = W) present two formula unit cells (AO_6 and BO_6) where BO_6 is characterized by zigzag chains of oxygen octahedral coordinating the metal ions (A^{2+}) and aligned along the z-axis [26]. They were carburized by TPRe method and tested in the hydrodenitrogenation (HDN) reaction. The samples pre- and post-HDN reaction were characterized by different techniques in order to find out the influence of the stoichiometric composition of the oxidic precursors on the phase distribution of W-based carbides and the catalytic performance.

2. Experimental

2.1. Carbide synthesis

The mixed oxides $Co_{1-x}Ni_xWO_4$ (x = 0, 0.25, 0.50, 0.75 and 1) were prepared by the organic matrix combustion synthesis using a stoichiometric proportion of cobalt (II) nitrate (CN) (Aldrich), nickel (II) nitrate (NiN) (BDH) and ammonium metatugstate (AMT) (Fluka Chemie) and double stoichiometric proportion of an organic matrix as fuel (urea). In a typical synthesis of $Co_{0.5}Ni_{0.5}WO_4$, a pyrex beaker (50 cm^3) containing a saturated aqueous mixture with molar proportion: 6CN:6NiN:1AMT:34urea was stirred to form a uniform mixture. The resulting jelly was combusted at 500 °C for 5 min in air to produce a voluminous material. The carburised catalysts were prepared using the temperature-programmed reaction (TPRe) method by carburising the mixed oxide material $Co_{1-x}Ni_xWO_4$ using a flow rate of 100 mL min^{-1} of a 10 vol.% C_2H_6/H_2 mixture. The temperature was increased linearly from room temperature to 700 °C at 1 °C min^{-1} and

held at 700 °C for 2 h. Then, the samples were quenched to room temperature under the carburisation mixture and passivated in a gentle 1% O_2/He flow for 24 h before exposure to the atmosphere.

2.2. Catalyst activity tests

The HDN reactions were carried out in a fixed-bed tubular quartz reactor (34 cm long, 4 mm i.d.) with an axial thermowell containing a thermocouple centred in the catalyst bed. A carbide sample (200 mg, <250 μm) was activated at 500 °C for 10 h using H_2 at a flow rate of 20 mL min^{-1} in order to remove residue material and the surface oxidic phases. Then, the temperature was lowered to 350 °C. The inlet gas was switched to H_2 saturated with pyridine vapour (99.9 Aldrich) at 0 °C (~0.75 kPa) and at a flow rate of 20 mL min^{-1}, the reaction pressure was 0.1 MPa. The products of reaction were analysed using an on-line HP 5890 Series II chromatograph equipped with a Hayesep R packed column (80–100 mesh, 3 m × 1/8″ × 2 mm SS) and a flame ionisation detector (FID). After completion of the catalytic reaction, the catalyst sample was cooled to room temperature under flowing argon and then passivated before exposure to the atmosphere.

2.3. Catalysts characterization

The analysis of the catalysts for carbon and nitrogen was carried out on the elemental analyser Vario EL. The samples were digested through oxidative combustion and the gases analysed with a thermal conductivity detector.

The crystalline phases of the oxidic precursors and the carburised catalysts before and after HDN reaction were identified by X-ray diffraction (XRD) using a Philips PW1710 diffractometer equipped with an X-ray tube (Cu Kα radiation λ = 1.5406 Å; 40 kV, 30 mA). The specimens were prepared by grinding small quantities of each sample in an agate mortar and pestle and then loaded into a flat sample holder. The data were collected at room temperature, in $\theta/2\theta$ reflection mode, scanning the specimens between 3° and 70° 2θ, using steps of 0.05°, with time per step of 1.25 s.

The different molybdenum species at local level of the oxidic precursors and the carburised catalysts were studied by laser Raman spectroscopy using a Yvon Jobin Labram spectrometer with a 632.8 nm HeNe, run in a back-scattered confocal arrangement. The samples were pressed in a microscope slide; the scanning time was set to 30 s. Raman spectra were recorded in air at room temperature with a resolution of 2 cm^{-1} and scanning range of 100–2500 cm^{-1}.

Thermogravimetric analysis (TGA) and differential scanning calorimetric (DSC) simultaneously in oxidative atmosphere or temperature-programmed oxidation (TPO) of the catalysts before HDN reaction was carried out on a Rheometric Scientific STA 1500 instrument. TGA-DSC profiles were done from room temperature to 750 °C on around 40–50 mg of sample loaded into a small alumina crucible using 25 mL min^{-1} of air and 10 °C min^{-1} of heating rate.

Transmission electron microscopy (TEM) was carried out using a JEOL 2000FX electron microscope with accelerating voltage of 200 kV. Mixed Co, Ni and W carbides before and after the HDN reaction were ground to a fine powder and dispersed in AR-grade chloroform. Then, they were placed in an ultrasonic bath for ca. 15 min. A drop of the suspension was put on a grid and positioned in the microscope specimen holder.

3. Results and discussion

3.1. Characterization of the oxidic precursors

Crystalline phase identification in the samples studied was carried out using the diffractometer analytical software after a revision of the PDF-ICDD database crystalline materials [27]. The X-ray powder diffraction patterns of catalyst precursors are shown in Fig. 1 with an expanded region from $29°$ up to $35°$ in 2θ at upper right side. The XRD patterns of $NiWO_4$ (PDF No. 72–1189) and $CoWO_4$ (PDF No. 72–0479) correspond to monoclinic crystalline structure of wolframite-type oxides. The patterns of the trimetallic oxides $Co_{1-x}Ni_xWO_4$ ($x = 0.25$, 0.5, 0.75) are similar to the patterns for $NiWO_4$ and $CoWO_4$, however the diffraction peaks show a clear shift to higher 2θ values with increasing of Ni content as shown in inset Figure. This shift is due to the shrinkage of the wolframite-structure unit cell when Co^{2+} ($R_{ionic} = 0.72$ Å) is substituted for Ni^{2+} ($R_{ionic} = 0.69$ Å) [28], indicating that a solid solution ($Co_{1-x}Ni_xWO_4$) is formed over the entire range of compositions. In addition, the diffraction peaks become more intense with the increasing of nickel content, probably due to the increase of the crystallite size and/or the crystalline degree of trimetallic oxide. In the XRD patterns, small and broad peaks characteristic of nickel oxide and tungsten trioxide are observed, suggesting that a small content of NiO and WO_3 do not fully react with CoO
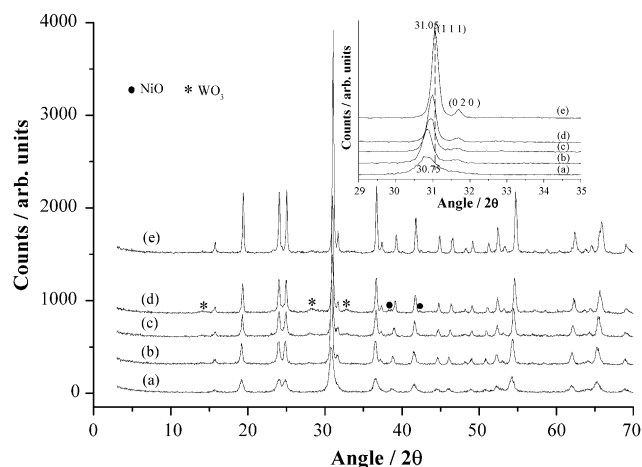

Fig. 1. X-ray diffraction patterns of the wolframite-type oxides of $Co_{1-x}Ni_xWO_4$: (a) $CoWO_4$, (b) $Co_{0.75}Ni_{0.25}WO_4$, (c) $Co_{0.50}Ni_{0.50}WO_4$, (d) $Co_{0.25}Ni_{0.75}WO_4$ and (e) $NiWO_4$. Inset: expanded region from $29°$ up to $35°$ in 2θ.
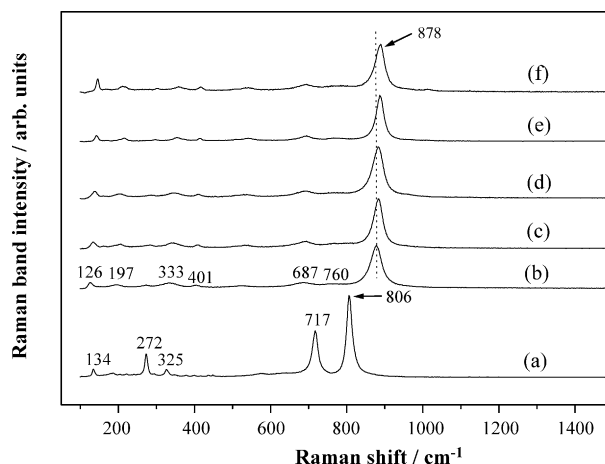
Fig. 2. Laser Raman spectra of the wolframite-type oxides of $Co_{1-x}Ni_x$ WO_4: (a) WO_3, (b) $CoWO_4$, (c) $Co_{0.75}Ni_{0.25}WO_4$, (d) $Co_{0.50}Ni_{0.50}WO_4$, (e) $Co_{0.25}Ni_{0.75}WO_4$ and (f) $NiWO_4$.

to produce the trimetallic oxide. However, no cobalt oxide is detected, probably due to the overlap of its diffraction peaks with the main crystalline phase.

The Raman spectra of the oxide precursors are given in Fig. 2. The spectrum of tungsten oxide is listed as reference. The major Raman bands of m-WO_3 (monoclinic structure) were seen at 806, 717 and 272 cm^{-1}, which correspond to the symmetric stretching, asymmetric stretching and deformation modes of the terminal W=O groups, respectively [29]. Other weak bands at 642, 573, 448, 326, 187 and 134 cm^{-1} are assigned to the vibrations of stretching, deformation and lattice modes. The spectrum of wolframite-type oxidic precursor $CoWO_4$ shows a strong Raman band at 878 cm^{-1} and a weak band around 760 cm^{-1}. They are due to the symmetric and asymmetric stretching modes of the terminal W=O bonds, as was described for the wolframite-type oxides $ZnWO_4$ [30] and $CdWO_4$ [30,31]. The weak Raman bands at 687 and 525 cm^{-1} are assigned to the vibration modes arising from the asymmetric and symmetric stretching of O—W—O bridges in the $(W_2O_4)_n$ polymeric chain, whereas the weak peaks at 401 and 333 cm^{-1} are tentatively assigned to the in-plane deformation and rotation modes of the W—O bonds (terminal and bridging), respectively [30,31]. The weak Raman band at 272 cm^{-1} is attributed to the vibration of Co—O stretching, whereas the small bands at 197 and 127 cm^{-1} might be due to out-of-plane and lattice modes [31]. The substitution of Co(II) by Ni(II) in the wolframite structure produces a clear shift of the Raman bands to higher wave number mainly due to an increase in W—O bond strength, which confirms the formation of the solid solution over the entire range of compositions as it was previously inferred by XRD.

3.2. Characterization of bimetallic and trimetallic W-based carbides

The oxidic precursors change from greenish-yellow to dark brown with increasing of Ni content and all the samples
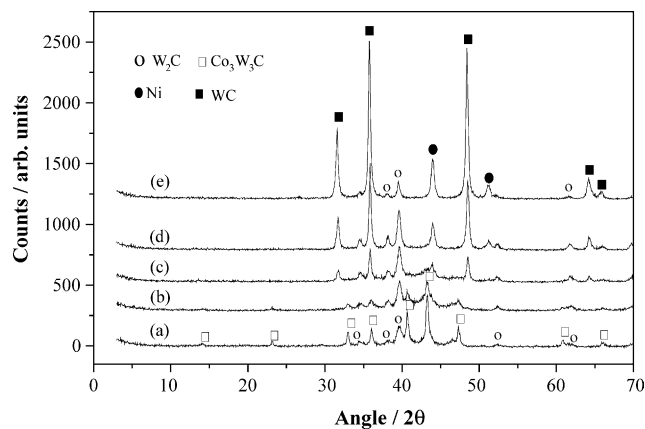
Fig. 3. X-ray diffraction patterns of the mixed Co, Ni and W carbide catalysts: (a) $CoWC_x$, (b) $Co_{0.75}Ni_{0.25}WC_x$, (c) $Co_{0.50}Ni_{0.50}WC_x$, (d) $Co_{0.25}Ni_{0.75}WC_x$ and (e) $NiWC_x$.

Fig. 4. Laser Raman spectra of the bimetallic and trimetallic Co, Ni and W carbide catalysts: (a) $CoWC_x$, (b) $Co_{0.75}Ni_{0.25}WC_x$, (c) $Co_{0.50}Ni_{0.50}WC_x$, (d) $Co_{0.25}Ni_{0.75}WC_x$ and (e) $NiWC_x$.

become black after the carburisation process. The XRD patterns of the resultant carbide materials are shown in Fig. 3. The $CoWC_x$ catalyst displays the diffraction peaks of the cubic bimetallic carbide Co_3W_3C (PDF No. 27–1125) and hexagonal close packed β-W_2C (PDF No. 79–0743) with an average nano-crystalline size of 26 nm, calculated using the main reflection peak. The addition of nickel decreases the content of the bimetallic carbide Co_3W_3C and favours the formation of the hexagonal structure α-WC (PDF No. 73–0471) and metal Ni. The samples $Co_{0.75}Ni_{0.25}WC_x$ and $Co_{0.50}Ni_{0.50}WC_x$ give broad diffraction peaks and a clear decrease in the peak intensities due to smaller crystallite size of the carbide materials (i.e., 20 nm). On the other hand, $Co_{0.25}Ni_{0.75}WC_x$ and $NiWC_x$ catalyst showed a notable increase of the average nano-crystalline size to 35 and 42 nm, respectively. The carbide samples showed a specific surface area into the range of 23–35 $m^2 g^{-1}$. These data clearly reveal that the used carburizing treatment is appropriate to prepare W-based carbides and also the phase distribution is strongly dependent on the wolframite-type mixed oxide composition.

The Raman spectra of the carbide materials and the total carbon content are shown in Fig. 4. The spectrum of the
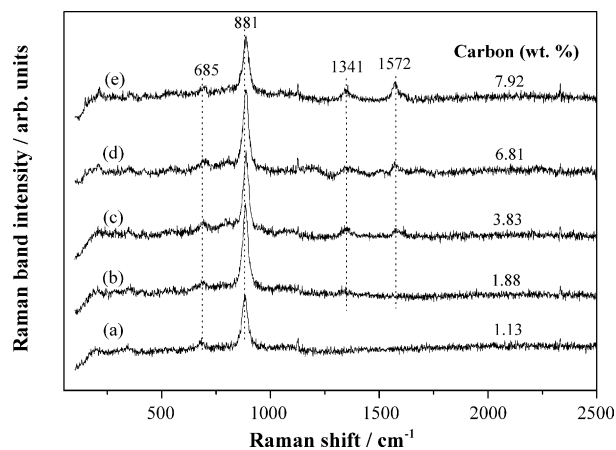
$CoWC_x$ catalyst clearly shows a strong Raman band at 881 cm^{-1} and weak band at 685 cm^{-1}, associated with the symmetric stretching mode of the terminal W=O groups and asymmetric stretching of the O−W−O bridges in the $(W_2O_4)_n$ polymeric chain, respectively [30,31], similar Raman bands were observed in the spectra of Ni-containing catalysts. The presence of mixed oxide coating at carbide surface has been also observed in the Co–Mo and Ni–W carbide catalysts and its formation was attributed to the passivation process [11,12]. The Ni-containing catalysts showed carbonaceous material owing to the high content of nickel, whose ability to facilitate the formation of carbon is well established [32]. The catalysts with Ni compositions greater than 0.25 display two Raman bands at 1572 and 1341 cm^{-1} assigned to the E_{2g} C−C stretching mode (G band) of graphitic carbon and A_{1g} disordered mode with basal plane dimension less than 200 Å (D band), respectively [33].

Representative TEM images of the trimetallic carbide catalysts are shown in Fig. 5. The micrograph of $CoWC_x$ shows an irregular morphology with large agglomerated carbide particles whereas $Co_{0.5}Ni_{0.5}WC_x$ was made up of smaller
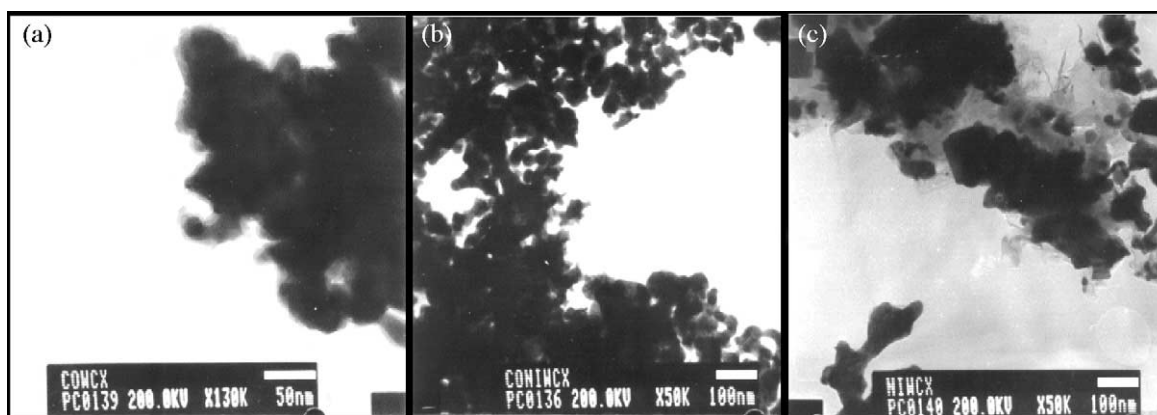

Fig. 5. TEM images of the of the mixed Co, Ni and W carbide catalysts: (a) $CoWC_x$, (b) $Co_{0.50}Ni_{0.50}WC_x$ and (c) $NiWC_x$.
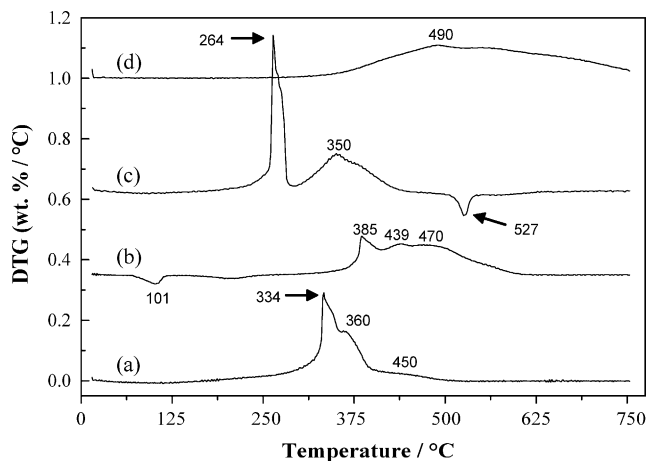
Fig. 6. Differential thermogravimetric analysis in air flow of single-phase samples: (a) β-W_2C, (b) α-WC, (c) Co_3W_3C and (d) CoC_x.

particles size, in line with the average crystalline size determined by XRD, with morphology fairly similar to the $CoWC_x$ catalyst. On the other hand, the $NiWC_x$ sample shows an irregular morphology and a broad particle size distribution. These TEM images clearly reveal that the molar Ni/Co ratio affects markedly the catalyst morphology and particle size of the carbide materials.

3.2.1. TG analysis of the carbide samples

Thermal gravimetric analysis (TGA) under flowing air was carried out on trimetallic, bimetallic and monometallic carbide samples. The differential TG (DTG) profiles of single-phase samples are displayed in Fig. 6. The TPO profile of β-W_2C shows three stages with total weight gain of 16.7 wt.%. The first step at 334 °C is tentatively assigned to the formation of tungsten oxycarbide ($W_2C_xO_y$) from the partial oxidation of ditungsten carbide, Fig. 6a. The oxycarbide phase has been observed during the oxidation of MeC (Me = Zr, Hf, Ti) [34] and the carburisation process of WO_3 [35] and MoO_3 [36] as precursor phase for the formation of final material. The second weight gains at 360 °C and third steps (broad and small state around 450 °C) correspond to the oxidation of that intermediate phase to tungsten oxide. The oxidation degree of β-W_2C to WO_3 was 0.76. This is obtained by dividing the measured weight gain with the theoretical one, which was calculated by assuming the complete conversion of β-W_2C to WO_3, according to the Eq. (1):

$$W_2C + 4O_2 \rightarrow 2WO_3 + CO_2 \tag{1}$$
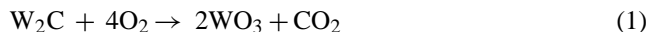
The 0.76 oxidation degree indicates an incomplete oxidation on the temperature range studied. Indeed, when one considers the formation of sub-oxide $WO_{2.5}$ an oxidation degree of 0.93 is achieved. This indicates the formation of non-stoichiometric $WO_{3-\lambda}$ or the homologous series W_nO_{3n-1} and W_nO_{3n-2} ($n \geq 4$), in which regions of corner-linked octahedral one separated from each other by short regions with a different structure giving a crystallographic shear (CS) plane [37].

The TPO profile for the α-WC compound displays a small weight loss (endothermic process) of 0.8 wt.% at 101 °C, which is associated with water desorption. At higher temperature regions there are three exothermic stages with a total weight gain of 17.4 wt.%, Fig. 6b. An oxidation degree of 0.95 suggests the formation of WO_3 as final product. On the other hand, the TPO profile for Co_3W_3C bimetallic carbide shows a total weight gain of 18.4 wt.% with an oxidation degree of 1.03 assuming a complete conversion of Co_3W_3C to a partially oxidized phase ($CoWO_3$). A weight loss of 2.5% at 527 °C is assigned to the oxidation of residual carbon material [34], Fig. 6c. Finally, the TPO profile for the cobalt carbide shows a broad stage with a maximum at 490 °C and weight gain of 30.9 wt.%. It is associated to the oxidation of CoC_x because the oxidation degree was 0.85, assuming the complete conversion of metal cobalt to Co_3O_4, Fig. 6d. Comparing the TPO profiles of the single-phase samples one can infer that the incorporation of cobalt into the W-based carbide lattice decreases significantly the oxidation temperature, probably due to descent of metal–carbon bond strength.

The TPO profiles for bimetallic and trimetallic Co, Ni and W carbides are displayed in Fig. 7. The $CoWC_x$ bimetallic catalyst presented three stages of 22.0 wt.% total weight gain and one weight loss of 1.9 wt.% at 523 °C (see Fig. 7a). The lower initial oxidation temperature compared with that of Co_3W_3C pure sample (Fig. 6c) might be attribute to the presence of an oxygen spill-over effect induced by carbon-deficient carbide (or intermetallic phase). The TPO profiles for the $Co_{0.75}Ni_{0.25}WC_x$ (22.2% total weight gain) and $Co_{0.50}Ni_{0.50}WC_x$ (18.9 wt.% total weight gain) catalysts showed an evident increase both in the oxidation temperature and in the number of oxidation steps compared with $CoWC_x$, due to the different crystalline phases present in those samples. The TPO profiles of the $Co_{0.25}Ni_{0.75}WC_x$ (17.3 wt.% total weight gain) and $NiWC_x$ (17.5 wt.% total weight gain)
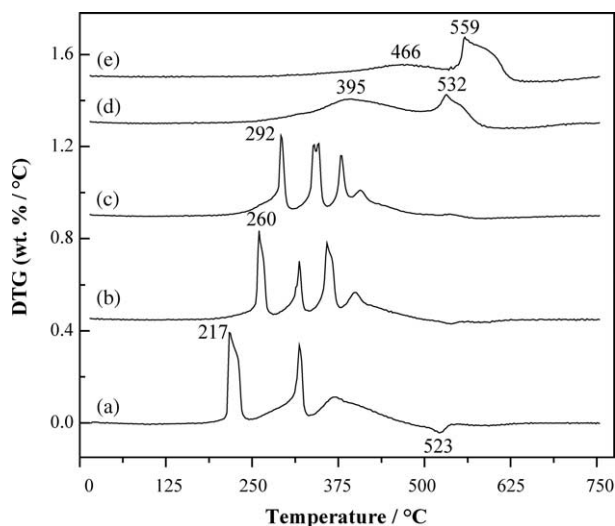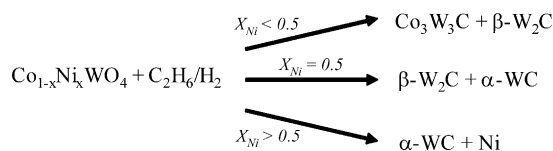

Fig. 7. Differential thermogravimetric analysis in air flow of the mixed Co, Ni and W carbide catalysts: (a) $CoWC_x$, (b) $Co_{0.75}Ni_{0.25}WC_x$, (c) $Co_{0.50}Ni_{0.50}WC_x$, (d) $Co_{0.25}Ni_{0.75}WC_x$ and (e) $NiWC_x$.

$$Co_{1-x}Ni_xWO_4 + C_2H_6/H_2 \xrightarrow{\begin{array}{c}X_{Ni} < 0.5\end{array}} Co_3W_3C + \beta\text{-}W_2C$$
$$\xrightarrow{X_{Ni} = 0.5} \beta\text{-}W_2C + \alpha\text{-}WC$$
$$\xrightarrow{X_{Ni} > 0.5} \alpha\text{-}WC + Ni$$

Scheme 1. Distribution of the major phases of mixed Co, Ni and W carbide catalysts.

show that the initial oxidation temperature further increases. They displayed a broad step due to the enrichment of α-WC as was determined by X-ray diffraction, whereas at higher temperature there was a step weight gain which is assigned mainly to the oxidation of metallic nickel. All the samples showed a 0.5–2.0% weight loss at temperatures greater than 500 °C associated with the oxidation of residual carbon material. The initial oxidation temperature markedly increases with the nickel loading, especially at high compositions (i.e., $X_{Ni} > 0.5$) when α-WC and also Ni are the main crystalline phases. This trend is in agreement with the higher initial oxidation temperature of α-WC compared with those of β-W_2C and Co_3W_3C (see Fig. 6).

From the aforementioned data and considering that at low content of Ni and/or Co these metals are well-dispersed on carbide surface the distribution of the major phases in function of Ni mole composition is summarized in Scheme 1.

The broad phase distribution with the metal composition might be mainly associated with diffusion limitations of carbon species within the oxidic precursor particles during the carburization process [38,39]. This seems to be a plausible reason when $X_{Ni} < 0.5$ but when nickel is greater than cobalt composition ($X_{Ni} > 0.5$) a high concentration of surface carbon (or CH_x species) at high carburization temperatures (i.e., 700 °C) might be the main driving force for the formation of the most thermodynamically stable α-WC from β-W_2C [40]. Indeed, it has been determined that this is a slow reaction and strongly dependent on PCH_4/PH_2 ratio [39], furthermore Xiao et al. [12] has recently shown that Ni decreases the carburization temperature of WO_3 to 630 °C and helps complete phase transformation from oxide to W_2C.

3.3. Catalyst performance and characterization after pyridine HDN reaction

The pyridine conversion and product distribution in the steady state are displayed in Fig. 8. $CoWC_x$ catalyst shows greater HDN activity that the Ni-containing carbide catalysts, whose activity did not change markedly with the nickel loading. The major products detected in gas phase were methane followed by C_2-C_4 and C_5, respectively. Nickel facilitates the formation of methane compared with the $CoWC_x$, which reflects the greater ability of the metallic particles (Ni) toward the catalytic hydrocracking reaction [32]. It is worth mentioning that the most active catalyst (i.e., $CoWC_x$) presented the lowest initial oxidation temperature, indicating that the carbon–metal bond strength play an important role in the catalytic process. However, this correlation was not observed for
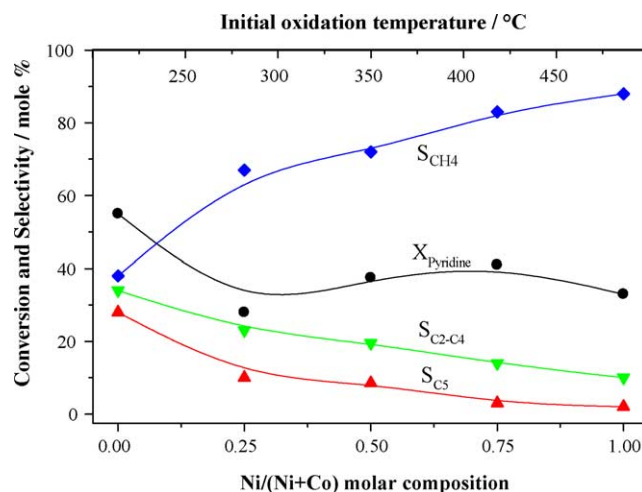
Fig. 8. Correlations of the pyridine conversion and products distribution with the Co, Ni and W carbide compositions and the initial oxidation temperature (catalytic reactions at 350 °C, $p = 0.1$ MPa, $v = 100$ mL $(g_{cat}\ min)^{-1}$).

the data of the Ni-containing catalysts. Indeed, as the Ni loading rises the initial oxidation temperature markedly increases, whereas the HDN activity was approximately constant. This strongly suggests that the nickel particles rather than α-WC control the catalytic behaviour of the Ni-containing catalysts.

The XRD patterns of the catalysts after pyridine-HDN reaction are illustrated in Fig. 9. The data indicate that post-HDN reaction catalysts have similar crystalline phases than those pre-HDN reaction samples. However, the diffraction peaks showed lower symmetric and intensity than those before HDN reaction. Comparing this data with the XRD patterns before HDN reaction (see Fig. 1), one can conclude that the catalysts underwent textural changes rather than structural modifications. Indeed, the average nano-crystallite size of the post-HDN reaction catalysts presented a reduction of 20–30% compared with the pre-HDN reaction catalysts in line with the increase of the specific surface areas (i.e., 63–115 m^2 g^{-1}) [41,42].
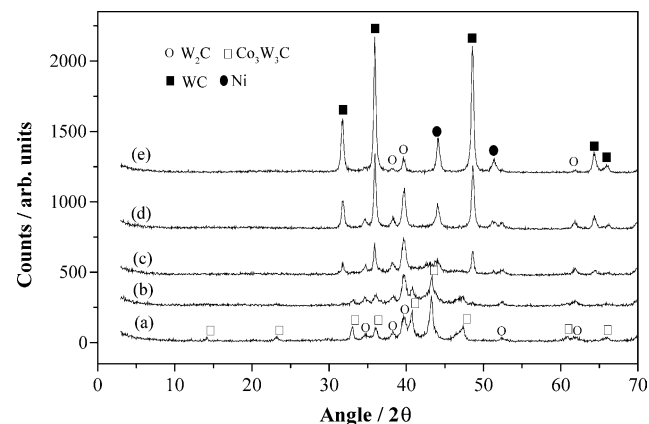
Fig. 9. X-ray diffraction patterns of the mixed Co, Ni and W carbide catalysts post-HDN reaction: (a) $CoWC_x$, (b) $Co_{0.75}Ni_{0.25}WC_x$, (c) $Co_{0.50}Ni_{0.50}WC_x$, (d) $Co_{0.25}Ni_{0.75}WC_x$ and (e) $NiWC_x$.
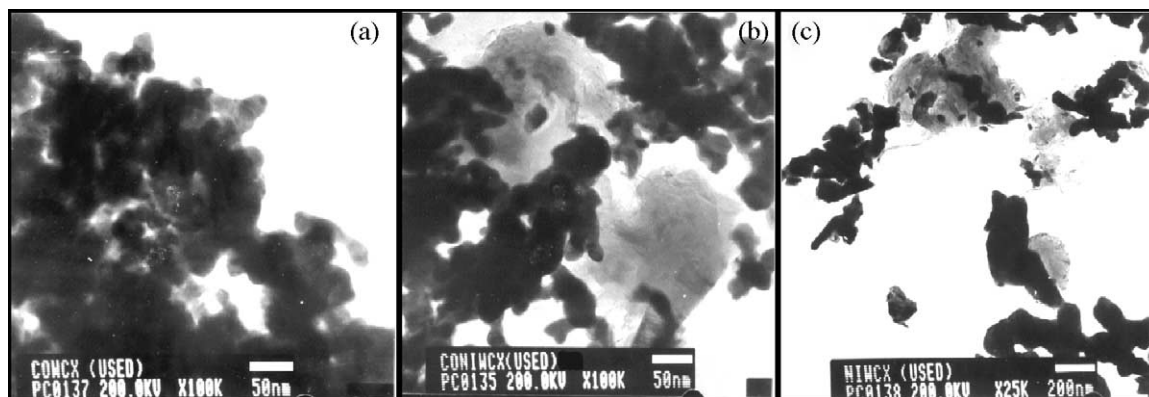
Fig. 10. TEM images of the bimetallic and trimetallic Co, Ni and W carbide catalysts after HDN reaction: (a) CoWC$_x$, (b) Co$_{0.50}$Ni$_{0.50}$WC$_x$ and (c) NiWC$_x$.

TEM images of the post-reaction carbide catalysts are shown in Fig. 10. The electron micrographs of the CoWC$_x$, Co$_{0.5}$Ni$_{0.5}$WC$_x$ and NiWC$_x$ catalysts display similar morphology to their corresponding pre-HDN catalysts, however the particle size decreased after the catalytic test in line with the data obtained by XRD. Amorphous graphitic carbon covers the small particles of the Ni-containing catalysts and nickel promotes carbon atoms diffusion or segregation at the catalyst surface, inhibiting the oxidic compound formation during the passivation process [41].

4. Concluding remarks

Urea-matrix combustion synthesis is a convenient method for preparing not only bimetallic, but also trimetallic wolframite-type mixed oxides (i.e., Co$_{1-x}$Ni$_x$WO$_4$) with a high purity and crystallinity degree. These mixed oxides can be used as precursors of W-based HDN carbide catalysts.

Temperature-programmed carburisation of Co$_{1-x}$Ni$_x$WO$_4$ using 10 vol.% C$_2$H$_6$/H$_2$ produced different crystalline phases, depending on the Ni/(Ni + Co) atomic ratio. At Ni compositions lower than Co contents the formation of Co$_3$W$_3$C and β-W$_2$C carbides is favoured, whereas at Ni compositions greater than those of Co the main phases were Ni and α-WC. The intermediate composition catalyst (Co$_{0.5}$Ni$_{0.5}$WC$_x$) showed a mixture of bimetallic and monometallic carbides. Small content of nickel when $X_{Co} > X_{Ni}$ or cobalt when $X_{Ni} > X_{Co}$ seem to be finally dispersed on the carbide surface.

The mixed Co, Ni and W carbides are active catalysts for pyridine HDN reaction. The CoWC$_x$ bimetallic catalyst showed greater activity in the steady state than Ni-containing catalysts. The morphology of the catalyst did not change during the catalytic reaction. The product distribution is strongly affected by the Ni/(Ni + Co) mole ratio. The Ni-containing catalysts showed higher selectivity to methane than the CoWC$_x$ catalyst whereas an opposite trend was observed for the production of C$_2$–C$_5$ hydrocarbons, mainly for C$_5$ compounds. It is envisaged that the HDN active phase present in CoWC$_x$ is different than that present in the Ni-containing catalysts and that carbon–metal bond strength, for the former, and metal nickel or weak Ni–C bond, for the latter, play a very important role in the catalytic process.

References

[1] F. Meunier, P. Delporte, B. Heinrich, Ch. Bouchy, C. Crouzet, C. Pham-Huu, P. Panissod, J.J. Lerou, P.L. Mills, M.J. Ledoux, J. Catal. 169 (1997) 33.

[2] R.J. O'Brien, L. Xu, X.X. Bi, P.C. Eklund, B.H. Davis, in: S.T. Oyama (Ed.), The Chemistry of Transition Metal Carbides and Nitrides Blackie, Academic & Professional, Glasgow, 1996, p. 362.

[3] L. Leclercq, M. Provost, H. Pastor, J. Grimblot, A.M. Hardy, L. Gengembre, G. Leclercq, J. Catal. 117 (1989) 371.

[4] D.A. White, S.M. Oleff, J.R. Fox, Adv. Ceram. Mater. 2 (1987) 53.

[5] R.B. Levy, M. Boudart, Science 181 (1973) 547.

[6] L. Volpe, M. Boudart, J. Solid State Chem. 59 (1985) 348.

[7] L. Volpe, M. Boudart, J. Solid State Chem. 59 (1985) 332.

[8] R. Kojima, K.-I. Aika, Appl. Catal. A: Gen. 219 (2001) 141.

[9] V. Schwartz, S.T. Oyama, J. Mol. Catal. A: Chem. 163 (2000) 269.

[10] T.-C. Xiao, A.P.E. York, H. Al-Megren, J.B. Claridge, H.-T. Wang, M.L.H. Green, C.R. Acad. Sci. 3 (2000) 451.

[11] T-C. Xiao, A.P.E. York, H. Al-Megren, V.C. Williams, H.-T. Wang, M.L.H. Green, J. Catal. 202 (2001) 100.

[12] T.-C. Xiao, H.-T. Wang, A.P.E. York, V.C. Williams, M.L.H. Green, J. Catal. 209 (2002) 318.

[13] P. Da Costa, C. Potvin, J.-M. Manoli, J.-L. Lemberton, G. Perot, G. Djéga-Mariadassou, J. Mol. Catal. A: Chem. 184 (2002) 323.

[14] K.R. McCrea, J.W. Logan, T.L. Tarbuck, J.L. Heiser, M.E. Bussell, J. Catal. 171 (1997) 255.

[15] K.Y. Park, W.K. Seo, J.S. Lee, Catal. Lett. 11 (1991) 349.

[16] J.S. Lee, S. Kim, Y.G. Kim, Top. Catal. 2 (1995) 127.

[17] A.P.E. York, J.B. Claridge, A.J. Brungs, S.C. Tsang, M.L.H. Green, Chem. Commun. (1997) 39.

[18] J.B. Claridge, A.P.E. York, A.J. Brungs, C. Márquez-Alvarez, J. Sloan, S.C. Tsang, M.L.H. Green, J. Catal. 180 (1998) 85.

[19] S.T. Oyama, C.C. Yu, S. Ramanathan, J. Catal. 184 (1999) 535.

[20] K.C. Patil, S.T. Aruna, S. Ekambaram, Curr. Opin. Solid State Mater. Sci. 2 (1997) 158.

[21] G. Xanthopoulou, G. Vekinis, Appl. Catal. B: Environ. 19 (1998) 37.

[22] G. Xanthopoulou, G. Vekinis, Appl. Catal. A: Gen. 199 (2000) 227.

[23] G. Xanthopoulou, Appl. Catal. A: Gen. 185 (1996) 185.

[24] P. Bera, K.C. Patil, V. Jayaram, G.N. Subbanna, M.S. Hegde, J. Catal. 196 (2000) 293.

[25] P. Bera, K.C. Patil, M.S. Hegde, Phys. Chem. Chem. Phys. 2 (2000) 3715.

[26] A.F. Wells, Structural Inorganic Chemistry, 4th ed., Clarendon press, London, 1975, p. 487.

[27] JCPDS Powder Diffraction File, International Centre for Diffraction Data, Swarthmore, PA, 1989.

[28] D.R. Lide (Ed.), CRC Handbook of Chemistry and Physics, 84th ed., CRC press, Boca Raton, 2003.

[29] M.F. Daniel, B. Desbat, J.C. Lassegues, B. Gerard, M. Figlarz, J. Solid State Chem. 67 (1987) 235.

[30] M. Crane, R.L. Frost, P.A. Williams, J.T. Kloprogge, J. Raman Spectrosc. 33 (2002) 62.

[31] M. Daturi, G. Busca, M.M. Borel, A. Leclaire, P. Piaggio, J. Phys. Chem. B 101 (1997) 4358.

[32] D.L. Trimm, Catal. Today 49 (1999) 3.

[33] D.S. Knight, W.B. White, J. Mater. Res. 4 (1989) 385.

[34] S. Shimada, Solid State Ionics 141/142 (2001) 99.

[35] T.-C. Xiao, A. Hanif, A.P.E. York, J. Sloan, M.L.H. Green, Phys. Chem. Chem. Phys. 4 (2002) 3522.

[36] A. Hanif, T.-C. Xiao, A.P.E. York, J. Sloan, M.L.H. Green, Chem. Mater. 14 (2002) 1009.

[37] L. Smart, E. Moore, Solid State Chemistry: An Introduction, Chapman & Hall, London, 1992.

[38] A. Löfberg, A. Frennet, G. Leclercq, L. Leclercq, J.M. Giraudon, J. Catal. 189 (2000) 170.

[39] J.-M. Giraudon, P. Devassine, J.-F. Lamonier, L. Delannoy, L. Leclercq, G. Leclercq, J. Solid State Chem. 154 (2000) 412.

[40] A. Hanif, D. Phil. Thesis, University of Oxford, 2000.

[41] S.L. González-Cortés, T.-C. Xiao, A.P.E. York, D. Ma, H. Al-Megren, M.L.H. Green, React. Kinet. Catal. Lett. 84 (2005) 1.

[42] H. Al-Megren, T.-C. Xiao, S.L. González-Cortés, S.H. Al-Khowaiter, M.L.H. Green, J. Mol. Catal. A: Chem. 225 (2005) 143.